Hindawi Publishing Corporation
Shock and Vibration
Volume 2015, Article ID 195682, 9 pages
http://dx.doi.org/10.1155/2015/195682

Research Article

Inverse Shape Reconstruction of Inner Cavities Using Guided SH-Waves in a Plate

Bin Wang,[1] Zhenghua Qian,[1] and Sohichi Hirose[2]

[1]*State Key Laboratory of Mechanics and Control of Mechanical Structures, Nanjing University of Aeronautics and Astronautics, 29 Yudao Jie, Nanjing 210016, China*
[2]*Department of Mechanical and Environmental Informatics, Tokyo Institute of Technology, 2-12-1 Ookayama, Meguro-ku, Tokyo 152-8552, Japan*

Correspondence should be addressed to Bin Wang; wangbin1982@nuaa.edu.cn

Received 24 December 2014; Accepted 16 February 2015

Academic Editor: Tony Murmu

Copyright © 2015 Bin Wang et al. This is an open access article distributed under the Creative Commons Attribution License, which permits unrestricted use, distribution, and reproduction in any medium, provided the original work is properly cited.

The paper proposes an inverse reconstruction method for inner cavities in a 2D plate using guided SH-waves. When a pure incident wave mode is sent toward the flaw area, reflected waves are observed at the far field due to mode conversion. From wave scattering theory, the reflected wave field is expressed by an integral over the unknown flaw surface concerning the total wave field. By the introduction of Born approximation and far-field expressions of Green's function, it is found that the reflection coefficient for the mode of the same order as that of the incident mode is related to the unknown shape of the cavity by Fourier transform relations. By mathematical deduction, we show that if the basic (0th-order) symmetric and the 1st-order antisymmetric modes are used as incident waves, the locations and shapes of upper and lower boundaries of the cavity can be reconstructed. Numerical examples are illustrated in the paper, and a proper condition for applying this method is discussed. The research can act as a basis of nondestructive inspection for latent flaws within more complicated structures.

1. Introduction

Ultrasonic guided waves have been widely used in nondestructive testing (NDT) for pipes, plate structures, and composite materials. Compared with bulk waves, they can travel over long distances and interrogate the whole cross section, which allow us to inspect a large range from a single access point [1]. The nondestructive testing methods using guided waves are based on the principle that when the incident wave is scattered from a flaw, a part of the energy is reflected back and the information of reflected wave is related to the location and size of the flaw.

Most researches on NDT concerning guided waves make use of signal-processing technology to analyze the time-of-flight (TOF) of reflected waves, in order to locate flaws within a plate, mostly surface defects or through holes. For example, Fromme et al. [2] and Rajagopalan et al. [3] used a single-transmitter-multireceiver configuration to inspect over a large span of the plate for defect locations and directivities using Lamb modes. Masserey and Fromme [4] used a simple pitch-catch device to detect the surface notch on a ribbed plate by Rayleigh-like waves. Hayashi and Murase [5] and Nishino et al. [6] also used torsional guided wave modes to detect flaws on a thin-wall pipe. Recently, Lee and Park [7] used pulsed laser to generate Lamb wave and a piezoelectric sensor to monitor the structure response and adopted wavenumber filtering to extract damage-sensitive features. Other researchers also tried tomographic approaches with the use of guided waves, such as [8–12]. Due to the complexity, fewer researches concern inspection of inner flaws using guided waves. Recently, Lee et al. [13] suggest a wavelet-transformed ultrasonic propagation imaging method to detect debondings in a sandwich plate. Watkins and Jha [14] proposed a modified time-reversal approach for detection of both inner and surface flaws in a plate using Lamb waves. Generally, the TOF-based methods can well detect the defects' positions and ranges; however, there are fewer researches available about reconstruction of flaws' exact shapes.

Recently, some researchers begin to make use of more information of reflected waves such as the amplitude and

phase for detailed flaw sizing and reconstruction, which is based on a better understanding of interaction between flaw and guided waves. A notable case is made by Singh et al. [15] and Castaings et al. [16] who studied flaw sizing in a 2D plate model. They used a finite-element-based model to calculate reflection coefficients for various values of flaw's geometric parameter, followed by an optimization process to match these values to coefficients induced by actual flaws. However, this method requires a basic knowledge of the flaw's location as a priori condition and needs excessive FEM modeling as a database. Wang et al. [17] studied the interaction between guided Lamb waves and internal rectangular defects by hybrid BEM formulation and pointed out that the variation of reflection or transmission coefficients with the defect's parameter can provide information for inverse reconstruction. Wang and Hirose also developed an inversion method based on wave scattering theory, using the reflection coefficients of guided SH-waves [18] and Lamb waves [19] to reconstruct the locations and shapes of surface thinning flaws.

In this paper, we propose an inverse reconstruction method for the location and shape of an inner cavity in a 2D isotropic plate, using ultrasonic guided SH-waves. This study is subsequent to the previous research on inverse analysis of shape reconstruction of surface flaws [18]. When a pure SH-wave mode is incident into the flaw zone, various reflected wave modes are generated and observed at the far field due to mode conversion. The reflection coefficients, defined by ratios between the amplitudes of the reflected waves and the incident wave, depend on the position and shape of the cavity. The cavity's position and shape can be defined by two functions, representing upper and lower boundaries of the cavity. On the basis of scattering theory, it is found that the two functions can be determined by the inverse Fourier transform of the reflection coefficients of 0th-order symmetric and 1st-order antisymmetric SH-wave modes, with the introduction of Born and far-field approximations. We will describe the problem statement in Section 2 and explain the formulation of the inverse reconstruction method in Section 3. Numerical examples are shown in Section 4 to illustrate validity of the inverse reconstruction method and discuss the proper application condition. This research provides a fast detection and reconstruction method for latent flaws inside plates using guided waves, which is especially useful when conventional point-to-point ultrasonic nondestructive inspection is unavailable. The current study also serves as a basis for theoretical research of NDT using more complex guided wave modes, such as Lamb waves, or its application in more complicated plate structures.

2. Problem Statement

We consider a 2D isotropic elastic plate with an inner elliptic cavity, as shown in Figure 1. The thickness of plate is $2b$. Two functions are defined to depict the inner cavity: the depth of the cavity's upper and lower boundaries from the upper surface, termed as $h(x_1)$ and $h'(x_1)$, respectively, and we define $t(x_1) = h'(x_1) - h(x_1)$.

Ultrasonic guided SH-waves, which have antiplane displacements in x_3-direction, are used for reconstruction of the inner cavity's location and shape. As shown in Figure 1, the incident guided SH-wave propagates from right to left along x_1-direction and is scattered by the cavity. The reflected wave is observed at the far field on the right side of the flaw area.

Suppose the incident wave is a pure guided SH-wave mode of nth-order with frequency ω, as shown by

$$u^{\text{inc}} = A_n^{\text{inc}} f_n(\beta_n x_2)\, e^{+i(\xi_n x_1 + \omega t)}. \tag{1a}$$

Here, $\beta_n = n\pi/2b$, $\xi_n = \sqrt{k^2 - \beta_n^2}$ is the longitudinal wavenumber, and $k = \omega/c_T$. $c_T = \sqrt{\mu/\rho}$ is the S-wave velocity of material, with μ being the shear stiffness and ρ the density of a plate. A_n^{inc} is the amplitude of the incident wave. $f_n(\beta_n x_2)$ is a trigonometric function defined as

$$f_n(\beta_n x_2) = \begin{cases} \cos(\beta_n x_2) & \text{for } n = 0, 2, 4, \ldots \text{ (symmetric mode)} \\ \sin(\beta_n x_2) & \text{for } n = 1, 3, 5, \ldots \text{ (antisymmetric mode)}. \end{cases} \tag{1b}$$

For convenience, the time factor $e^{+i\omega t}$ in wave fields will be omitted in the following context.

Due to mode conversion, various SH-waves, including propagating and nonpropagating modes, can be excited by the scatterer as the incident wave hits the cavity. However, as the observation position is far away from the flaw area, nonpropagating modes decay and the reflected wave u^{ref}, which is received from the incident side, is composed of only propagating modes, as illustrated by the following equation:

$$u^{\text{ref}} = \sum_m A_m^{\text{ref}} f_m(\beta_m x_2)\, e^{-i\xi_m x_1}, \tag{2}$$

where A_m^{ref} is the amplitude of the mth wave mode and summation m is taken for all the propagating modes travelling from left to right.

These modes are orthogonal with each other on a cross section of a plate, which was proved by Auld [20]. If there are two modes termed N and M, propagating with wavenumbers k_N and k_M, respectively, for the case of SH-wave, the orthogonality has the following formation:

$$\int_{-b}^{b} (u_N \tau_M^* - \tau_N u_M^*)\, dx_2 = V(N)\, \delta_{NM}, \tag{3}$$

where u_I and τ_I are the modal displacement and shear stress τ_{13} of the mode I. The asterisk symbol means complex conjugate. δ_{NM} is taken as unit when $N = M$ and zero otherwise, and $V(N)$ is the integral value when $M = N$. If the mode is normalized, $V(N) = i$.

Therefore, using the orthogonality, we can obtain the amplitude A_m^{ref} by the following equation:

$$A_m^{\text{ref}} = \frac{\int_{-b}^{b} \left(u^{\text{ref}} \tau_m^* - u_m^* \tau^{\text{ref}}\right) dx_2}{\int_{-b}^{b} (u_m \tau_m^* - u_m^* \tau_m)\, dx_2}, \tag{4}$$

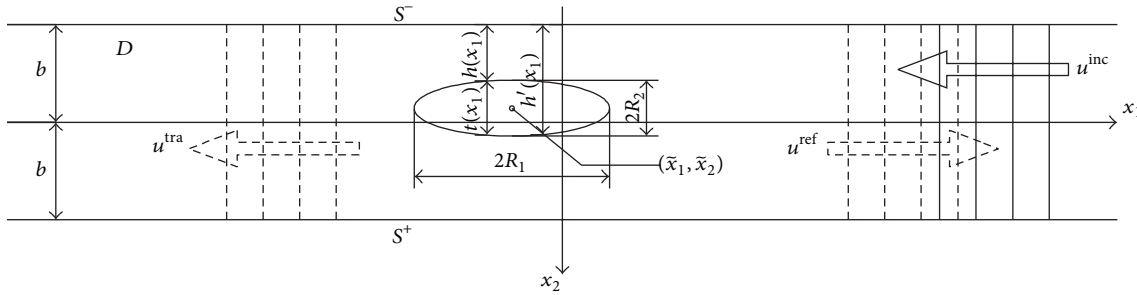

Figure 1: Schematic of the inverse problem.

where u^{ref} and τ^{ref} represent overall displacement and stress of the reflected wave field. In numerical calculations, (4) is adopted to separate each mode from one another. While in experimental studies, various separation methods are used, for example, 2D Fourier transform in [21], application of Bragg grating sensor in [22], and mode compensation method in [23].

The aim of inverse reconstruction is to find the location and shape of the inner cavity. Mathematically, it is the process of reconstructing functions $t(x_1)$ and $h(x_1)$, using the reflection coefficients A_m^{ref} as input data.

3. Inverse Reconstruction Procedure

The formulation of inverse reconstruction method is based on the integral expression for the scattered wave by the inner cavity. The scattered wave field at the observation point $\mathbf{X}$ can be expressed by an integral over the surface of cavity S, as shown by (5). If $\mathbf{X}$ is located at the incident side (as the situation discussed here), the scattered wave observed is also the reflected wave. Consider

$$\begin{aligned} u^{\text{sca}}(\mathbf{X}) &= u^{\text{ref}}(\mathbf{X}) \\ &= \int_S \left[\mu \frac{\partial U(\mathbf{x}-\mathbf{X})}{\partial x_k} n_k u^{\text{tot}}(\mathbf{x}) \right. \\ &\qquad \left. -\mu \frac{\partial u^{\text{tot}}(\mathbf{x})}{\partial x_k} n_k U(\mathbf{x}-\mathbf{X}) \right] dS(\mathbf{x}), \end{aligned} \tag{5}$$

where u^{sca} (u^{ref}) is the displacement of scattered (reflected) wave at observation point $\mathbf{X}$, $u^{\text{tot}} = u^{\text{inc}} + u^{\text{sca}}$ is the total displacement on the cavity surface S, and n_k is the unit normal vector pointing outward.

In (5), $U(\mathbf{x}-\mathbf{X})$ is Green's function for SH-wave in a plate waveguide, which has been obtained by Hirose [24] in an integral form. If the observation point is far away from the flaw area, the far-field expression of Green's function can be deduced as follows:

$$\begin{aligned} U(\mathbf{x}-\mathbf{X}) \approx & -\frac{i}{4b\mu\xi_0} e^{-i\xi_0|x_1-X_1|} \\ & -\sum_j \frac{i}{2b\mu\xi_j} f_j(\beta_j x_2) f_j(\beta_j X_2) e^{-i\xi_j|x_1-X_1|}, \end{aligned} \tag{6}$$

where f_j is a trigonometric function defined by (1b).

As shown by (6), it is seen that far-field Green's function can be expressed as the combination of different modes of guided SH-waves. The first term on the right-hand side of (6) is the fundamental (0th symmetric) mode, and the summation index j is taken for all the propagating symmetric and antisymmetric modes.

If the wavelength of an incident wave is much larger than the size of the cavity, the magnitude of scattered displacement is much less than that of the incident wave, due to weak scattering by a cavity. Then, the total wave field u^{tot} is replaced by incident wave field u^{inc}, which is known as Born approximation. Applying Gauss's theory, we can transfer the surface integral into the volume integral:

$$\begin{aligned} u^{\text{ref}}(\mathbf{X}) = \mu \int_V \left[-k^2 u^{\text{inc}}(\mathbf{x}) U(\mathbf{x}-\mathbf{X}) \right. \\ \left. + \frac{\partial u^{\text{inc}}(\mathbf{x})}{\partial x_k} \frac{\partial U(\mathbf{x}-\mathbf{X})}{\partial x_k} \right] dV(\mathbf{x}). \end{aligned} \tag{7}$$

As mentioned in the previous section, we firstly assume that the incident wave is a single fundamental (0th symmetric) SH-mode, propagating from right to left side in Figure 1, and the reflected wave is observed at the far field on the right side of the cavity. Also, by mode separation, the portion of the same mode as the incident wave is obtained.

In this situation, the displacement field of incident wave is written as (8), and Green's function corresponding to the fundamental SH-mode is expressed as (9). Consider

$$u^{\text{inc}}(\mathbf{x}) = A_0^{\text{inc}} e^{+ikx_1}, \tag{8}$$

$$U(\mathbf{x}-\mathbf{X}) = -\frac{i}{4\mu bk} e^{+ik(x_1-X_1)}. \tag{9}$$

Substituting (8) and (9) into (7) and taking the limit of $X_1 \to \infty$, the reflected wave of the 0th symmetric mode u_0^{ref} is written as

$$u_0^{\text{ref}}(\mathbf{X}) = \frac{ikA_0^{\text{inc}}}{2b} \int_V e^{+2ikx_1} dV(\mathbf{x}) \cdot e^{-ikX_1} \equiv A_0^{\text{ref}} e^{-ikX_1}. \tag{10a}$$

The volume integral in (10a) becomes

$$\int_V e^{+2ikx_1} dV(\mathbf{x}) = \int_{-\infty}^{\infty} \int_{h(x_1)}^{h(x_1)+t(x_1)} dx_2 e^{+2ikx_1} dx_1 = \int_{-\infty}^{\infty} t(x_1) e^{+2ikx_1} dx_1. \tag{10b}$$

Thus, we have the following Fourier transform relation:

$$C_0^{\text{ref}}(k) \equiv \frac{A_0^{\text{ref}}}{A_0^{\text{inc}}} = \frac{ik}{2b} \int_{-\infty}^{\infty} t(x_1) e^{+2ikx_1} dx_1, \tag{11a}$$

$$t(x_1) = \frac{b}{i\pi k} \int_{-\infty}^{\infty} C_0^{\text{ref}}(k) e^{-2ikx_1} d(2k), \tag{11b}$$

where the reflection coefficient C_0^{ref} is defined as the quotient of amplitudes for reflected wave over the incident wave, which is a function of wavenumber k. From (11b), the function $t(x_1)$ is obtained.

Secondly, the vertical location $h(x_1)$ of the cavity is determined by using the reflection coefficient of higher-order SH-wave mode. If the incident wave and the reflected wave are single mth-order ($m \geq 1$) SH-wave mode (symmetric or antisymmetric), the displacement of incident wave and corresponding Green's function are expressed by the following equations:

$$u^{\text{inc}}(\mathbf{x}) = A_m^{\text{inc}} f_m\left(\frac{m\pi x_2}{2b}\right) e^{+i\xi_m x_1}, \tag{12}$$

$$U(\mathbf{x}-\mathbf{X}) = -\frac{i}{2\mu b \xi_m} f_m\left(\frac{m\pi x_2}{2b}\right) f_m\left(\frac{m\pi X_2}{2b}\right) e^{+i\xi_m(x_1-X_1)}, \tag{13}$$

where guided wavenumber for the mth-order SH-mode is $\xi_m = \sqrt{k^2 - (m\pi/2b)^2}$.

Substituting (13) into (7), we have (14) which resembles (10a) and (10b):

$$\begin{aligned} u_m^{\text{ref}}(\mathbf{X}) &= \frac{iA_m^{\text{inc}}}{2b} \int_V \left[\xi_m + (-1)^m \frac{k^2}{\xi_m} \cos\left(\frac{m\pi x_2}{b}\right)\right] e^{+2i\xi_m x_1} dV(\mathbf{x}) \cdot f\left(\frac{m\pi X_2}{2b}\right) e^{-i\xi_m X_1} \\ &\equiv A_m^{\text{ref}} f\left(\frac{m\pi X_2}{2b}\right) e^{-i\xi_m X_1}, \end{aligned} \tag{14}$$

where $f(x)$ is the trigonometric function defined by (1b). By defining $C_m^{\text{ref}}(\xi_m) = A_m^{\text{ref}}/A_m^{\text{inc}}$ and rewriting the volume integral as a double integral, we have

$$\begin{aligned} C_m^{\text{ref}}(\xi_m) &\equiv \frac{A_m^{\text{ref}}}{A_m^{\text{inc}}} \\ &= \frac{i}{2b} \int_{-\infty}^{\infty} \int_{-b+h(x_1)}^{-b+h(x_1)+t(x_1)} \left[\xi_m + (-1)^m \frac{k^2}{\xi_m} \cos\left(\frac{m\pi x_2}{b}\right)\right] \cdot e^{+2i\xi_m x_1} dx_2 dx_1 \\ &= \frac{i}{2b} \int_{-\infty}^{\infty} \left[\xi_m t(x_1) + (-1)^m \frac{bk^2}{m\pi\xi_m} \cdot \left(\sin\frac{m\pi}{b}(h(x_1) - b + t(x_1)) - \sin\frac{m\pi}{b}(h(x_1) - b)\right)\right] e^{+2i\xi_m x_1} dx_1. \end{aligned} \tag{15}$$

It is noticed that the integral of the first item in the square bracket over x_1, that is, $(i\xi_m/2b) \int_{-\infty}^{\infty} t(x_1) e^{+2i\xi_m x_1} dx_1$, is equal to $C_0^{\text{ref}}(\xi_m)$ as seen in (11a). Thus, we can simplify (15) into

$$\begin{aligned} &(-1)^m \frac{ik^2}{2m\pi\xi_m} \int_{-\infty}^{\infty} \left[\sin\frac{m\pi}{b}(h(x_1) - b + t(x_1)) - \sin\frac{m\pi}{b}(h(x_1) - b)\right] e^{+2i\xi_m x_1} dx_1 \\ &= C_m^{\text{ref}}(\xi_m) - C_0^{\text{ref}}(\xi_m). \end{aligned} \tag{16}$$

The integrand $F(x_1) \equiv \sin(m\pi/b)(h(x_1) - b + t(x_1)) - \sin(m\pi/b)(h(x_1) - b)$ in (16) can be obtained by performing the inverse Fourier transform of the coefficient $C_m^{\text{ref}}(\xi_m) - C_0^{\text{ref}}(\xi_m)$:

$$F(x_1) = (-1)^{m-1} \cdot \frac{im\xi_m}{k^2} \int_{-\infty}^{\infty} \left[C_m^{\text{ref}}(\xi_m) - C_0^{\text{ref}}(\xi_m)\right] e^{-2i\xi_m x_1} d(2\xi_m). \tag{17}$$

The function $h(x_1)$ is obtained by solving the transcendental equation as follows:

$$F(x_1) = \sin\frac{m\pi}{b}(h(x_1) - b + t(x_1)) - \sin\frac{m\pi}{b}(h(x_1) - b). \tag{18}$$

However, it should be noted that, within the definition range of $-b \leq h(x_1) \leq b$, (18) has multiple solutions. The larger m is, the more roots it has. To avoid too many "virtual images" of the cavity, we choose $m = 1$ (1st-order antisymmetric mode). In this case, $h(x_1)$ has two solutions between $-b$ and b, which means a "real image" and a "virtual image" of the cavity are formed by the inversion process.

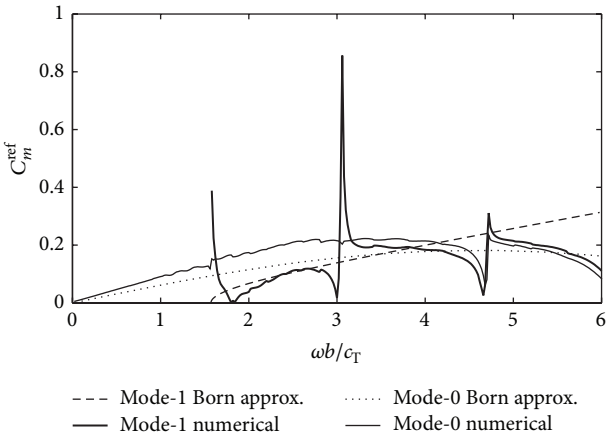

Figure 2: Reflection coefficients for $R_1 = R_2 = 0.2b$, $\widetilde{x}_2 = -0.5b$.

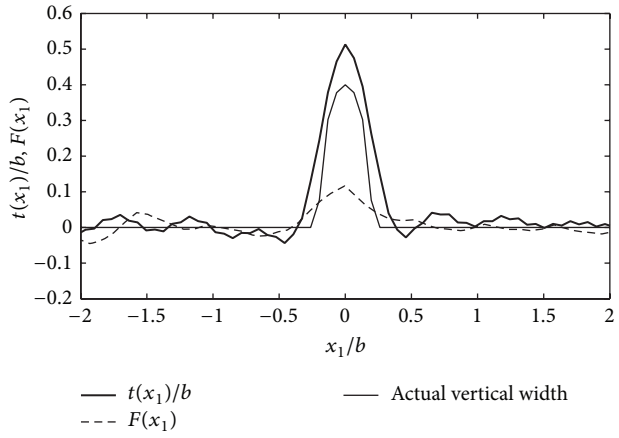

Figure 3: Reconstructed $t(x_1)$ and $F(x_1)$ for $R_1 = R_2 = 0.2b$, $\widetilde{x}_2 = -0.5b$.

4. Numerical Examples

For numerical verifications of the proposed inverse method, the reflection coefficients of 0th-order symmetric and 1st-order antisymmetric guided SH-wave modes due to various elliptic cavities are calculated by the means of mode-exciting method [25] and are used as input data in the inverse analysis.

The geometry of an elliptic cavity is given by the horizontal length $2R_1$and vertical length $2R_2$, as well as the center location $(\widetilde{x}_1, \widetilde{x}_2)$. The first example is the reconstruction of a circular cavity with the radius of $R_1 = R_2 = 0.2b$ and the center location $(0, -0.5b)$, using guided SH-waves. In (11b) and (17), the integration range is taken from $-\infty$ to $+\infty$. For numerical calculation, we consider a large frequency upper limit Ω, and consequently the numerical integral range for ξ_m is $(-\Xi_m, +\Xi_m)$, where $\xi_m = \sqrt{(\omega/c_T)^2 - (m\pi/2b)^2}$, $\Xi_m = \sqrt{(\Omega/c_T)^2 - (m\pi/2b)^2}$, $(m = 0, 1)$. Here, we set $\Omega b/c_T = 7.0$. We also let $C_n^{\text{ref}}(\xi_m) = C_n^{\text{ref}*}(-\xi_m)$, $(m, n = 0, 1)$, where the asterisk symbol means complex conjugate. Figure 2 shows the absolute values of the reflection coefficients $|C_m^{\text{ref}}|$ versus the normalized frequency $\omega b/c_T$ of mth-order guided SH-wave modes ($m = 0$ or 1). As a reference, the reflection coefficients estimated by Born approximation given by (15) are also drawn in Figure 2.

Table 1 illustrates the validation chart of the obtained reflection and transmission coefficients at different frequency points. The coefficients C_{AaBb} are defined as the quotient of amplitudes of reflected/transmitted waves over the incident wave (see Table 1). Two relations are used for validation. Firstly, due to energy conservation, the sum of the squares of reflection coefficients plus that of transmitted coefficients should be 1. Secondly, because the flaw is symmetric, for incident waves excited from the right side and the left side, their reflection/transmission coefficients should have the same absolute value.

Table 1 lists the situation where 1 or 2 modes exist in the waveguide at the given frequency. The cases where higher-order modes exist are also checked. From "energy check" in Table 1, it is seen that the energy conservation is satisfied. From the "relative error" column, we can notice that most of relative errors do not exceed 5%, while the biggest one occurs where nominator is very small, so the absolute error is also not large.

Substituting these coefficients into (11b) and (17), the function $t(x_1)$ and the intermediate function concerning flaw position information $F(x_1)$ are obtained, as shown by Figure 3. The function of position $h(x_1)$ can be determined by solving (18), after determining the functions $F(x_1)$ and $t(x_1)$. Ideally, for intact parts with no flaw, $t(x_1)$ is zero, and to obtain $h(x_1)$ is meaningless. However, as seen in Figure 3, the function $t(x_1)$ is not zero even in the nonflaw region because of errors in inversion. Therefore, in this study, a flaw region is defined as the area where $t(x_1)$ shows values larger than 25% of the maximum value of $t(x_1)$, and the upper boundary coordinate $h(x_1)$ is calculated only within the flaw region. By determining the functions of $t(x_1)$ and $h(x_1)$, the upper and lower boundaries of the cavity can be obtained and the image of the cavity is reconstructed.

In Figure 4, the reconstructed upper and lower boundaries are shown with thick curves and the shape of the original circular flaw is shown with thin curves. The "actual" reconstructed image is shown in solid curves, and the "virtual" one is illustrated in dashed curves, which appears at the mirror image position against the "actual" image. The inverse method is furthermore applied to other cavities at different locations and with different sizes. Figures 5 and 6 illustrate the reconstructed boundaries of the circular cavities with the radius of $R_1 = R_2 = 0.2b$ and center locations $(0, -0.7b)$ and $(0, 0)$, respectively. Figures 7–11 show the results for elliptic cavities with different combinations of the radii R_1 and R_2, while the center location $(\widetilde{x}_1, \widetilde{x}_2)$ of elliptic cavities is kept at $(0, -0.5b)$ for all the cases.

From Figures 4–6, it can be seen that the shapes of cavities are fairly well reconstructed, regardless of different vertical positions of a flaw. In Figure 6, we can see that as the cavity's center is on the x_1-axis, the "actual" and "virtual" images overlap each other.

The results of reconstructed cavities with different elliptic radiuses are twofold. In the cases of $R_1 = 0.1b$, $0.05b$

Table 1: An illustration of validation chart for reflection and transmission coefficients.

Freq.	Number of modes	Ref. or tra. coefficients inc. wave from left	Ref. or tra. coefficients inc. wave from right	Relative error of coefficients for inc. wave from left and right
0.1	1	$\lvert C_{1111}\rvert = 0.011441611$	$\lvert C_{2121}\rvert = 0.011441611$	0
		$\lvert C_{1121}\rvert = 0.999934543$	$\lvert C_{2111}\rvert = 0.999934543$	0
		Energy check: $\sum \lvert C_{11Ab}\rvert^2 = 1.000$	Energy check: $\sum \lvert C_{21Ab}\rvert^2 = 1.000$	
2.0	2	$\lvert C_{1111}\rvert = 0.174070111$	$\lvert C_{2121}\rvert = 0.174910464$	0.48%
		$\lvert C_{1112}\rvert = 0.162546674$	$\lvert C_{2122}\rvert = 0.161951563$	0.37%
		$\lvert C_{1121}\rvert = 0.971008475$	$\lvert C_{2111}\rvert = 0.970534705$	0.049%
		$\lvert C_{1122}\rvert = 0.02974192$	$\lvert C_{2112}\rvert = 0.02468971$	16%
		$\lvert C_{1211}\rvert = 0.162862467$	$\lvert C_{2221}\rvert = 0.162771155$	0.056%
		$\lvert C_{1212}\rvert = 0.038026818$	$\lvert C_{2222}\rvert = 0.037097031$	2.5%
		$\lvert C_{1221}\rvert = 0.026354694$	$\lvert C_{2211}\rvert = 0.027964747$	6.1%
		$\lvert C_{1222}\rvert = 0.985423619$	$\lvert C_{2212}\rvert = 0.985802799$	0.038%
		Energy check: $\sum \lvert C_{11Ab}\rvert^2 = 1.000463866$ $\sum \lvert C_{12Ab}\rvert^2 = 0.999724501$	Energy check: $\sum \lvert C_{21Ab}\rvert^2 = 0.999369174$ $\sum \lvert C_{21Ab}\rvert^2 = 1.000459824$	

Definition of coefficients is as follows.
Suppose the mth mode is used as the incident wave; then, we introduce the direction numbers,
1: the left direction of the flaw, 2: the right direction,
and the reflection/transmission coefficients C_{AaBb}.
Meanings of subindices:
C_{AaBb}: A-incident direction ($A = 1,2$); a-incident mode order; B-scattered direction ($B = 1,2$); b-scattered mode order (A and B the same: reflection coefficient; A and B different: transmission coefficient).
Wave field:
$u^{\text{inc}} = A_m^{\text{inc}} f_m(\beta_m x_2) e^{\pm i\xi_m x_1}$ (+ for incident wave from 2; − from 1);
$u^{\text{ref}} = \sum_n A_n^{\text{ref}} f_n(\beta_n x_2) e^{\mp i\xi_n x_1}$ (− for reflected wave to 2; + to 1);
$u^{\text{tra}} = \sum_k A_k^{\text{tra}} f_k(\beta_k x_2) e^{\pm i\xi_k x_1}$ (+ for transmitted wave to 1; − to 2).
The coefficients are defined as
$C_{2m2n}(C_{1m1n}) = A_n^{\text{ref}}/A_m^{\text{inc}}$ (reflection coefficient);
$C_{2m1k}(C_{1m2k}) = A_k^{\text{tra}}/A_m^{\text{inc}}$ (transmission coefficient).

and $R_2 = 0.2b$, as seen in Figures 7 and 8, respectively, the vertical positions of upper and lower boundaries are well found, but the flaw ranges in x_1-direction are enlarged compared to reality. In general, for a flaw shape with rapid change in x_1-direction, high-frequency components of reflection coefficients are needed to obtain good accuracy in shape reconstruction. However, in our approach, only relatively low-frequency components are available because Born approximation is appropriate in the low-frequency zone. That is why we cannot reconstruct images for narrow flaws as shown by Figures 7 and 8 with fine resolution.

On the other hand, in the cases of $R_1 = 0.3b$ and $0.5b$, as shown by Figures 9–11, respectively, the ranges of flaw area in x_1-direction agree well with the actual locations, whereas the positions of upper and lower boundaries are deviated from the reality, especially for the case of $R_1 = 0.5b$ and $R_2 = 0.2b$. The reasons may be stated as follows.

In Figure 12, the absolute values of reflection coefficients in the case of $R_1 = 0.5b$ and $R_2 = 0.2b$ are illustrated. We can see that, for the 0th SH-wave mode, the reflection coefficients given by Born approximation are close to the numerical results, whereas, for the 1st-order SH-wave mode, the differences between numerical reflection coefficients and Born approximation values become very large, especially within some frequency bands; for example, $\omega b/c_T = 1.5\sim2.0$ and $2.5\sim3.0$. The large reflection coefficients are due to structural resonance. If the cavity is relatively long in x_1-direction and close to the surface, the region between the cavity boundary and the plate surface behaves like a thin "plate" supported by elastic ends, which can vibrate in large amplitude near its resonance frequencies. In this case, the cavity can be seen as a strong scatterer and Born approximation is not valid anymore. On the other hand, the reflection coefficients for the 0th-order SH-wave mode still match Born approximation values. Consequently, the function $t(x_1)$ is still well reconstructed, but the reconstructed $h(x_1)$ deviates from reality. As a comparison, for the case of $R_1 = R_2 = 0.2b$, as shown in Figure 2, it is seen that the reflection coefficients given by Born approximation are close to numerical values for both 0th- and 1st-order wave modes, except at some limited points which are cutoff frequencies of other wave modes. Thus, both functions $t(x_1)$ and $h(x_1)$ are well reconstructed.

In a summary, the applicability of Born approximation, which is accurate for low-frequency components and for weak scatterers, is the key factor for the accuracy of the proposed reconstruction method. The accuracy of the inversion method depends on the size and location of the cavity. If the cavity's dimension in x_1-direction R_1 is relatively large and

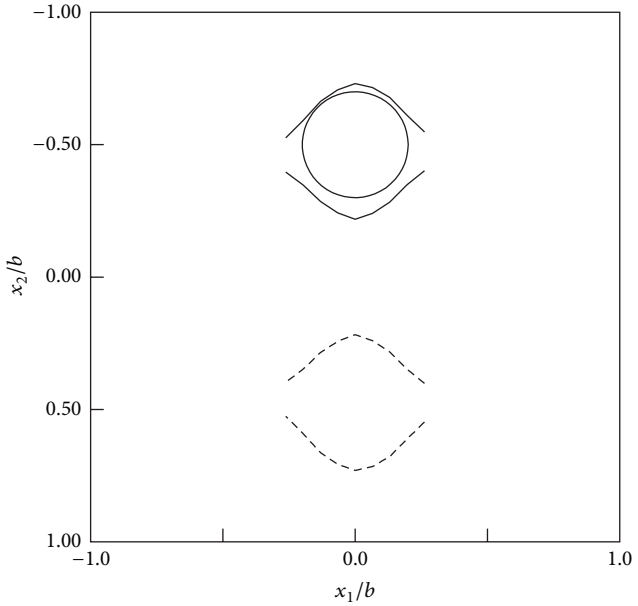

Figure 4: Reconstructed cavity with $R_1 = R_2 = 0.2b$, $\widetilde{x}_2 = -0.5b$.

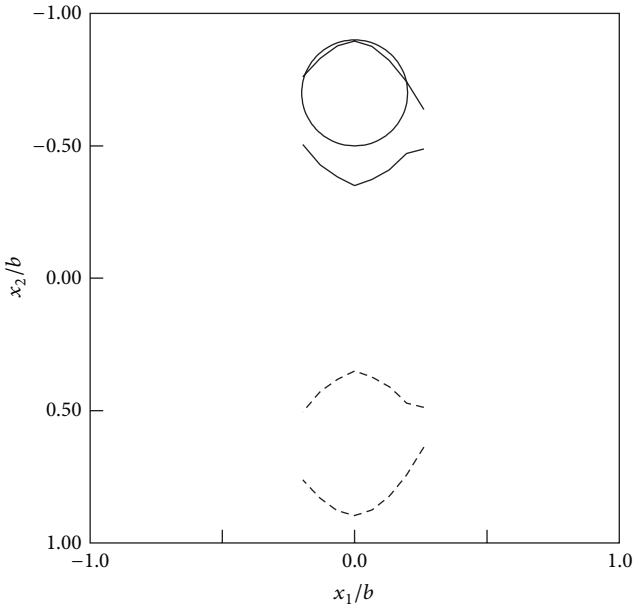

Figure 5: Reconstructed cavity with $R_1 = R_2 = 0.2b$, $\widetilde{x}_2 = -0.7b$.

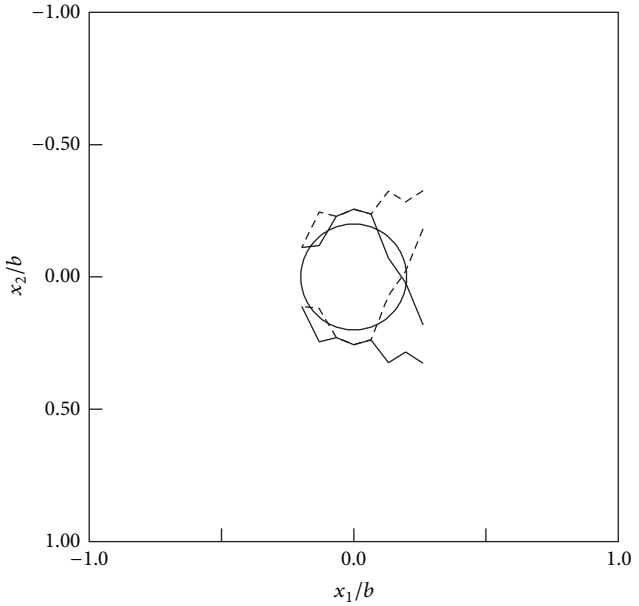

Figure 6: Reconstructed cavity with $R_1 = R_2 = 0.2b$, $\widetilde{x}_2 = 0.0$.

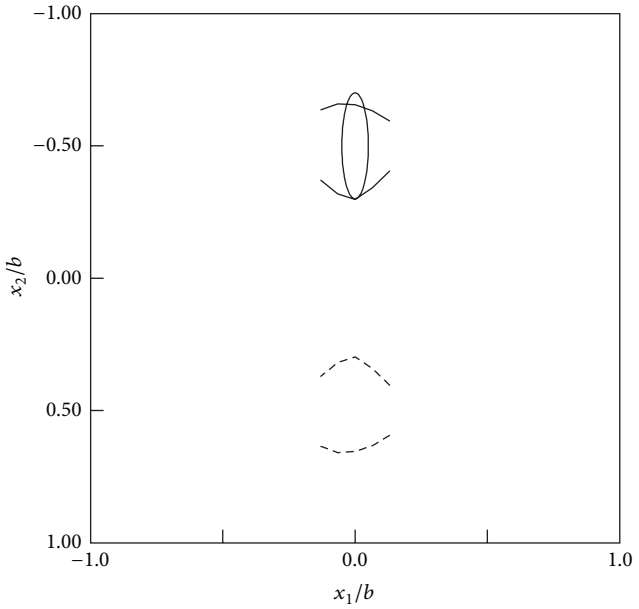

Figure 7: Reconstructed cavity with $R_1 = 0.05b$, $R_2 = 0.2b$, and $\widetilde{x}_2 = -0.5b$.

the cavity is close to the surface of plate, due to structural resonance, the reflection coefficients for 1st-order SH-wave mode cannot be well estimated by Born approximation, which makes the function $h(x_1)$ lose accuracy. On the other hand, if R_1 is relatively small, $t(x_1)$ changes rapidly on x_1-direction, and after Fourier transform it contains high-frequency components that cannot be covered by low-frequency Born approximation. As a result, the boundaries in x_1-direction tend to be vaguer.

5. Conclusion

In this paper, a new inverse reconstruction method for inner cavities in a 2D plate using guided SH-wave has been proposed. The location and shape of unknown cavities have been reproduced by performing inverse Fourier transforms of reflection coefficients of both 0th-order symmetric and 1st-order antisymmetric SH-wave modes in frequency domain.

The validity of this method was illustrated by numerical examples. If the dimensions of cavity in x_1- and x_2-directions are within an appropriate range, the image of the cavity can

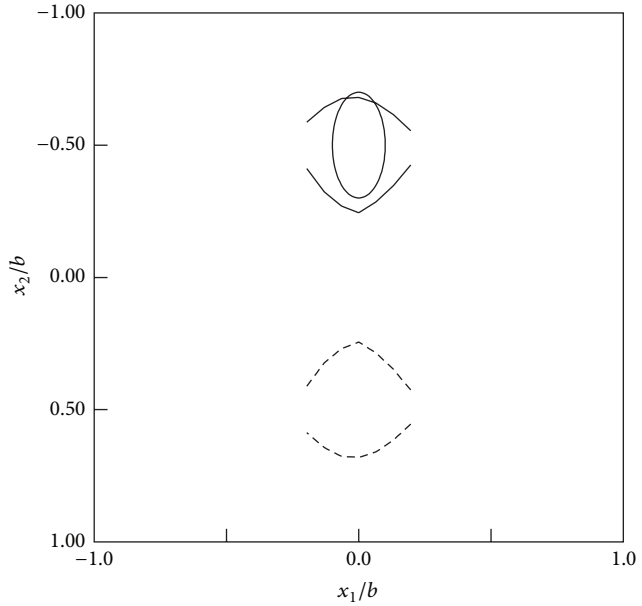

Figure 8: Reconstructed cavity with $R_1 = 0.1b$, $R_2 = 0.2b$, and $\tilde{x}_2 = -0.5b$.

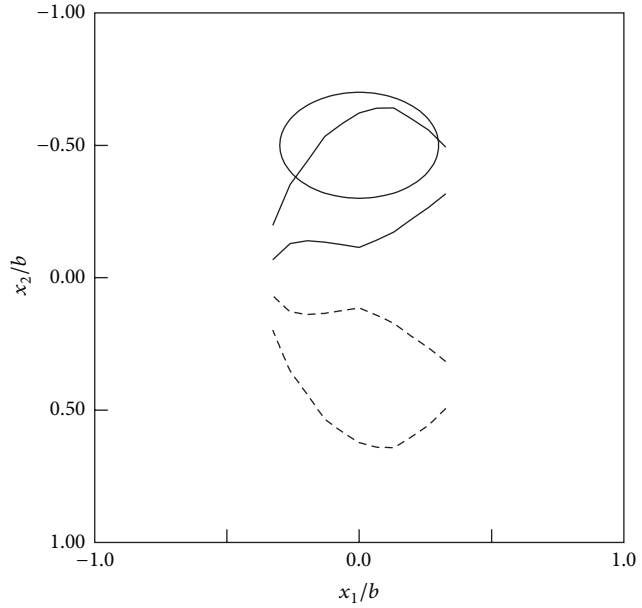

Figure 9: Reconstructed cavity with $R_1 = 0.3b$, $R_2 = 0.2b$, and $\tilde{x}_2 = -0.5b$.

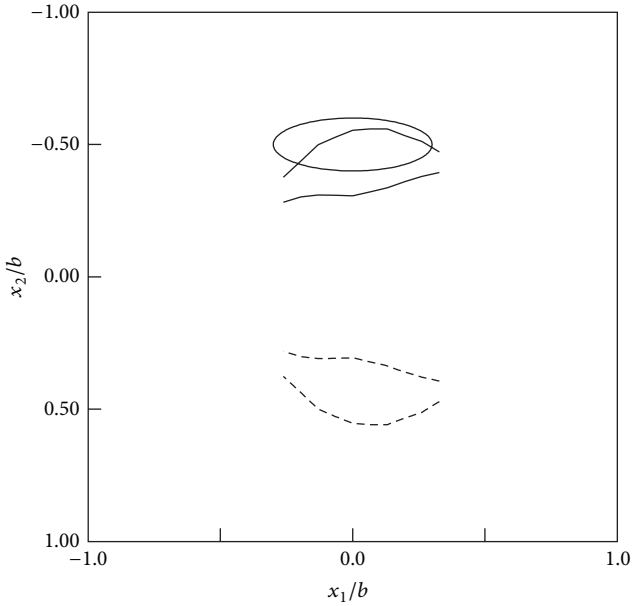

Figure 10: Reconstructed cavity with $R_1 = 0.3b$, $R_2 = 0.1b$, and $\tilde{x}_2 = -0.5b$.

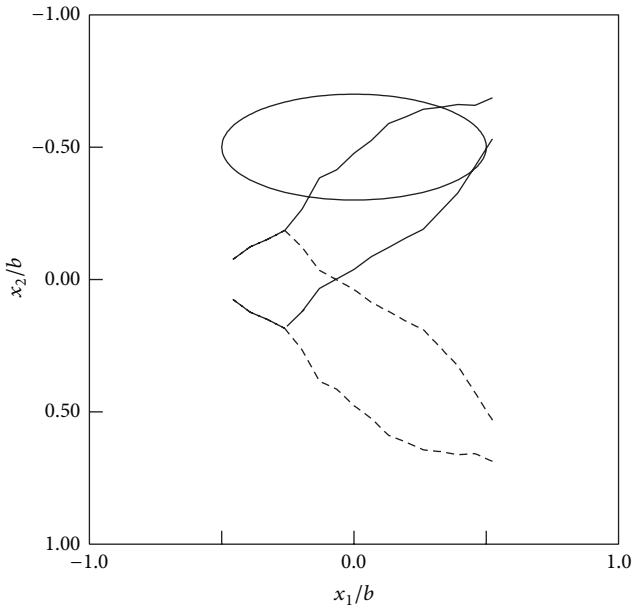

Figure 11: Reconstructed cavity with $R_1 = 0.5b$, $R_2 = 0.2b$, and $\tilde{x}_2 = -0.5b$.

be well reconstructed. Because of the applicable condition of Born approximation, the accuracy of reconstruction depends on horizontal size and location of cavity. If the cavity's dimension is relatively wide in x_1-direction and close to the plate surface, Born approximation no longer holds for 1st-order SH-wave mode because of structural resonance; thus, the reconstructed position in x_2-direction loses accuracy. If the cavity is narrow in x_1-direction, the low-frequency limitation of Born Approximation makes the boundary of flaw image vaguer.

For further research, we hope to improve the method and apply it for reconstruction of inner holes in a realistic 3D plate model. Experimental studies, followed by field applications, will also be investigated in the future.

Conflict of Interests

The authors declare that there is no conflict of interests regarding the publication of this paper.

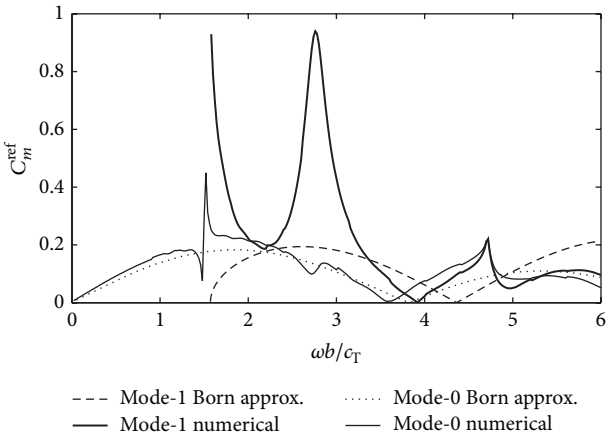

FIGURE 12: Reflection coefficients for $R_1 = 0.5b$, $R_2 = 0.2b$, and $\tilde{x}_2 = -0.5b$.

Acknowledgments

This work was supported by the National Natural Science Foundation of China (Grant no. 51405225), the Program for New Century Excellent Talents in Universities (Grant no. NCET-12-0625), the Natural Science Foundation for Distinguished Young Scholars of Jiangsu Province (Grant no. BK20140037), and the Natural Science Foundation of Jiangsu Province (Grant no. BK20140808). Additional supports also come from Fundamental Research Funds for Central Universities and Priority Academic Program Development of Jiangsu Higher Education Institutions (PAPD).

References

[1] J. L. Rose, "A baseline and vision of ultrasonic guided wave inspection potential," *Journal of Pressure Vessel Technology, Transactions of the ASME*, vol. 124, no. 3, pp. 273–282, 2002.

[2] P. Fromme, P. D. Wilcox, M. J. S. Lowe, and P. Cawley, "On the development and testing of a guided ultrasonic wave array for structural integrity monitoring," *IEEE Transactions on Ultrasonics, Ferroelectrics, and Frequency Control*, vol. 53, no. 4, pp. 777–784, 2006.

[3] J. Rajagopalan, K. Balasubramaniam, and C. V. Krishnamurthy, "A single transmitter multi-receiver (STMR) PZT array for guided ultrasonic wave based structural health monitoring of large isotropic plate structures," *Smart Materials and Structures*, vol. 15, no. 5, pp. 1190–1196, 2006.

[4] B. Masserey and P. Fromme, "Surface defect detection in stiffened plate structures using Rayleigh-like waves," *NDT and E International*, vol. 42, no. 6, pp. 564–572, 2009.

[5] T. Hayashi and M. Murase, "Defect imaging with guided waves in a pipe," *Journal of the Acoustical Society of America*, vol. 117, no. 4, pp. 2134–2140, 2005.

[6] H. Nishino, K. Ogura, T. Komatsu, and K. Yoshida, "Defect detection of a pipe using a guided wave generated by an efficient transduction with a reflector," *Japanese Journal of Applied Physics*, vol. 48, no. 9, Article ID 094501, 2009.

[7] C. Lee and S. Park, "Flaw imaging technique for plate-like structures using scanning laser source actuation," *Shock and Vibration*, vol. 2014, Article ID 725030, 14 pages, 2014.

[8] E. V. Malyarenko and M. K. Hinders, "Ultrasonic Lamb wave diffraction tomography," *Ultrasonics*, vol. 39, no. 4, pp. 269–281, 2001.

[9] H. Gao, Y. Shi, and J. L. Rose, "Guided wave tomography on an aircraft wing with leave in place sensors," in *Review of Quantitative Nondestructive Evaluation*, D. O. Thompson and D. E. Chimenti, Eds., vol. 24, pp. 1788–1794, American Institution of Physics, Denver, Colo, USA, 2005.

[10] T. R. Hay, R. L. Royer, H. Gao, X. Zhao, and J. L. Rose, "A comparison of embedded sensor Lamb wave ultrasonic tomography approaches for material loss detection," *Smart Materials and Structures*, vol. 15, no. 4, pp. 946–951, 2006.

[11] P. Huthwaite and F. Simonetti, "High-resolution guided wave tomography," *Wave Motion*, vol. 50, no. 5, pp. 979–993, 2013.

[12] P. Huthwaite, "Evaluation of inversion approaches for guided wave thickness mapping," *Proceedings of the Royal Society A: Mathematical, Physical and Engineering Sciences*, vol. 470, no. 2166, Article ID 20140063, 2014.

[13] J.-R. Lee, C. Ciang Chia, H. Jin Shin, C.-Y. Park, and D. Jin Yoon, "Laser ultrasonic propagation imaging method in the frequency domain based on wavelet transformation," *Optics and Lasers in Engineering*, vol. 49, no. 1, pp. 167–175, 2011.

[14] R. Watkins and R. Jha, "A modified time reversal method for Lamb wave based diagnostics of composite structures," *Mechanical Systems and Signal Processing*, vol. 31, pp. 345–354, 2012.

[15] D. Singh, M. Castaings, and C. Bacon, "Sizing strip-like defects in plates using guided waves," *NDT & E International*, vol. 44, no. 5, pp. 394–404, 2011.

[16] M. Castaings, D. Singh, and P. Viot, "Sizing of impact damages in composite materials using ultrasonic guided waves," *NDT and E International*, vol. 46, no. 1, pp. 22–31, 2012.

[17] S. Wang, S. Huang, and W. Zhao, "Simulation of Lamb wave's interactions with transverse internal defects in an elastic plate," *Ultrasonics*, vol. 51, no. 4, pp. 432–440, 2011.

[18] B. Wang and S. Hirose, "Inverse problem for shape reconstruction of plate-Thinning by guided SH-Waves," *Materials Transactions*, vol. 53, no. 10, pp. 1782–1789, 2012.

[19] B. Wang and S. Hirose, "Shape reconstruction of plate thinning using reflection coefficients of ultrasonic lamb waves: a numerical approach," *ISIJ International*, vol. 52, no. 7, pp. 1328–1335, 2012.

[20] B. A. Auld, *Acoustic Fields and Waves in Solids*, vol. 2, John Wiley & Sons, New York, NY, USA, 1973.

[21] D. Alleyne and P. Cawley, "A two-dimensional Fourier transform method for the measurement of propagating multimode signals," *Journal of the Acoustical Society of America*, vol. 89, no. 3, pp. 1159–1168, 1991.

[22] N. Rajic, C. Davis, and A. Thomson, "Acoustic-wave-mode separation using a distributed Bragg grating sensor," *Smart Materials and Structures*, vol. 18, no. 12, Article ID 125005, 2009.

[23] K. Xu, D. Ta, P. Moilanen, and W. Wang, "Mode separation of Lamb waves based on dispersion compensation method," *The Journal of the Acoustical Society of America*, vol. 131, no. 4, pp. 2714–2722, 2012.

[24] S. Hirose, "SH wave scattering by a defect in a plate," in *Review of Quantitative Nondestructive Evaluation*, D. O. Thompson and D. E. Chimenti, Eds., vol. 17, pp. 73–80, Plenum, New York, NY, USA, 1998.

[25] A. Gunawan and S. Hirose, "Mode-exciting method for Lamb wave-scattering analysis," *Journal of the Acoustical Society of America*, vol. 115, no. 3, pp. 996–1005, 2004.

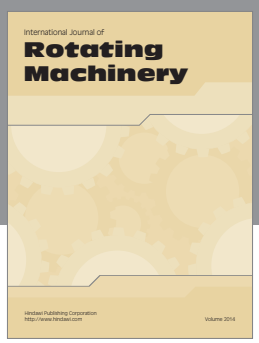

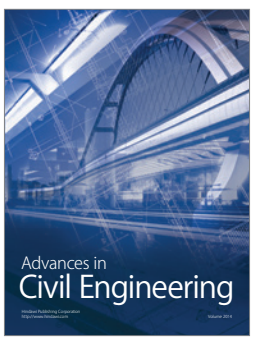

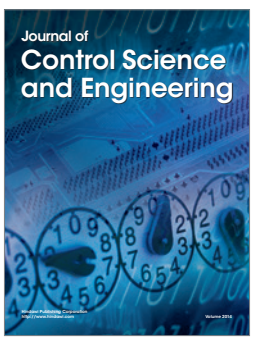

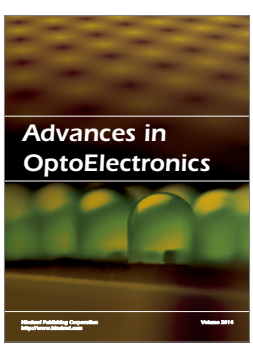

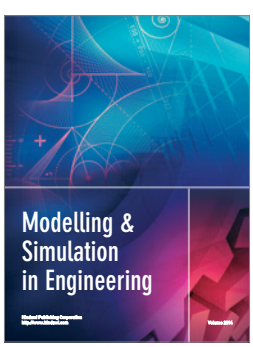

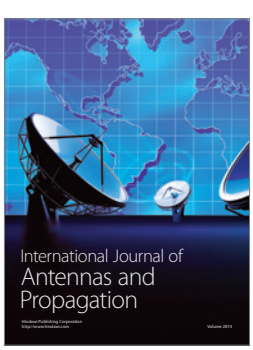

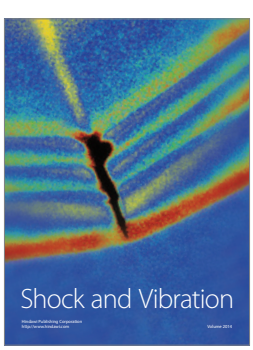

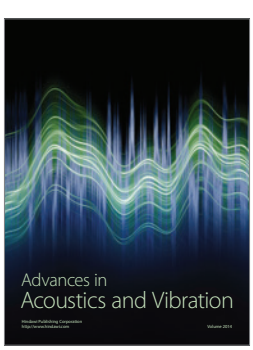

Hindawi

Submit your manuscripts at
http://www.hindawi.com